IEICE TRANS. COMMUN., VOL.E83–B, NO.2 FEBRUARY 2000

PAPER

Analysis of Elliptical Microstrip Antennas with and without a Circular Slot

Takafumi FUJIMOTO†, **Kazumasa TANAKA**†, *and* **Mitsuo TAGUCHI**†, *Members*

SUMMARY The wall admittance of an arbitrarily shaped microstrip antenna is generally formulated. As examples, elliptical microstrip antennas with and without a circular slot are calculated. The wall admittance is determined by the spectral domain analysis in order to consider the effect of the dielectric substrate. The electromagnetic fields within the cavity are expanded in terms of the eigenfunctions in the cylindrical coordinate system and their expansion coefficients are determined by applying the impedance boundary condition at the aperture in the sense of the least squares. The calculated input impedance and axial ratio agree fairly well with the experimental data. The proposed method is valid for the microstrip antennas with a patch whose geometry deviates from the particular coordinate system, such as single-feed circularly polarized microstrip antennas.

key words: *microstrip antenna, wall admittance, spectral domain, cavity model, least squares*

1. Introduction

In the analysis of a microstrip antenna (MSA) by the cavity model [1], MSA is divided into two regions. The inside region of the cavity is assumed as the region enclosed above and below by the conducting plates and on the side by the admittance wall. The other is the outside region of the cavity. The electromagnetic fields within the cavity are expanded in terms of the eigenfunctions. Their expansion coefficients are determined by the impedance boundary condition at the side aperture. The contribution from the outside region of the cavity is taken into account by the wall admittance at the aperture. The accuracy of wall admittance depends on the analytical model of the outside region of the cavity and affects the resonant frequency and the input impedance of MSA. The wall admittances have been investigated for MSA with a patch of simple configuration, such as rectangular MSA [2]–[4], circular MSA [5]–[7] and circular ring MSA [7], [8].

The authors have proposed the formulation method for the wall admittance of arbitrarily shaped MSA and calculated the circular MSA as an example [9]. The wall admittance in [9] is defined by the magnetic field produced by the equivalent magnetic current on the aperture from the continuity condition on the tangential component of the magnetic field on the aperture. The outside region of the cavity is modeled as a layered medium consisting of the free space, the dielectric substrate with a magnetic dipole and the ground plane. The magnetic field is derived using Green's functions obtained by the spectral domain analysis. The wall conductance obtained by the spectral domain analysis includes the conductance due to the surface wave. The contribution of the surface wave conductance to the wall conductance is significant around the resonant frequency of the first mode and at higher frequencies. The contribution increases as the dielectric constant and thickness of the substrate increase. The method of moments in the spectral domain is often applied to an arbitrarily shaped MSA [10]. The proposed method is simpler than the method of moments in the spectral domain because it is not necessary to solve the integral equation for unknown electric currents on the patch. The calculated input impedances agree fairly well with the experimental data for the dielectric substrate thickness up to 0.048 λ_g (λ_g is the wavelength within the dielectric at the resonant frequency of MSA).

In this paper, the wall admittance of the arbitrarily shaped MSA proposed in [9] is generalized and the elliptical MSAs with and without a circular slot are calculated. Most single-feed circularly polarized MSAs have a patch whose geometry deviates from the particular coordinate system. In this paper, a cavity model applicable to such MSAs is proposed. Shen represented the electromagnetic fields within the cavity of the elliptical MSA in terms of Mathieu functions and used the wall admittance of the circular MSA [11]. In this paper, the electromagnetic fields within the cavity of the elliptical MSAs with and without a circular slot are expanded in terms of the eigenfunctions in the cylindrical coordinate system, which are more easily treated compared with Mathieu functions. Their expansion coefficients are determined by applying the impedance boundary condition at the apertures in the sense of the least squares [12]. In order to ascertain the validity of the proposed method, the calculated input impedance and axial ratio are compared with the experimental data.

2. Fields within Cavity

Figure 1 shows the geometry and coordinate system of an arbitrarily shaped MSA. The radius of the circumscribed circle of the patch is a_0 and that of the inscribed circle of the slot is a_1. The relative dielectric constant

Manuscript received February 1, 1999.
Manuscript revised June 24, 1999.

†The authors are with the Department of Electrical and Electronic Engineering, Faculty of Engineering, Nagasaki University, Nagasaki-shi, 852-8521 Japan.

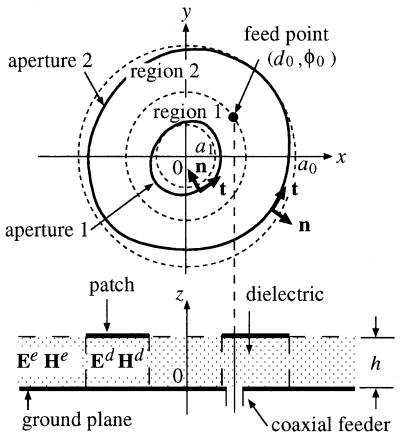

Fig. 1 Geometry of arbitrarily shaped MSA.

and thickness of the substrate are ε_r and h, respectively. The antenna is excited at $r = d_0$, $\phi = \phi_0$ by a coaxial feeder through the dielectric substrate. $\mathbf{n}$ and $\mathbf{t}$ are the unit normal vector outward from the aperture and the tangential vector along the aperture. The electromagnetic fields within and outside the cavity are denoted by $\mathbf{E}^d$, $\mathbf{H}^d$ and $\mathbf{E}^e$, $\mathbf{H}^e$, respectively.

The thickness of the substrate is assumed to be much smaller than the wavelength, so the electromagnetic fields within the cavity do not vary along the z direction. The electric field within the cavity $\mathbf{E}^d$ is expressed in terms of the eigenfunctions in the cylindrical coordinate system (r, ϕ, z) as

$$\mathbf{E}^d = E_z^d \mathbf{i}_z = \sum_{n=0}^{N} (E_{zn}^{cJ} + E_{zn}^{sJ} + E_{zn}^{cN} + E_{zn}^{sN}) \mathbf{i}_z \quad (1)$$

In Region 1 $\quad (a_1 \le r \le d_0)$

$$E_{zn}^{cJ} = A_n J_n(k_1 r) \cos(n\phi) \quad (2)$$

$$E_{zn}^{cN} = B_n N_n(k_1 r) \cos(n\phi) \quad (3)$$

$$E_{zn}^{sJ} = C_n J_n(k_1 r) \sin(n\phi) \quad (4)$$

$$E_{zn}^{sN} = D_n N_n(k_1 r) \sin(n\phi) \quad (5)$$

In Region 2 $\quad (d_0 \le r \le a_0)$

$$E_{zn}^{cJ} = F_n J_n(k_1 r) \cos(n\phi) \quad (6)$$

$$E_{zn}^{cN} = G_n N_n(k_1 r) \cos(n\phi) \quad (7)$$

$$E_{zn}^{sJ} = K_n J_n(k_1 r) \sin(n\phi) \quad (8)$$

$$E_{zn}^{sN} = L_n N_n(k_1 r) \sin(n\phi) \quad (9)$$

where $k_1 = \omega\sqrt{\mu_0 \varepsilon_1} = \omega\sqrt{\mu_0 \varepsilon_r \varepsilon_0}$. $J_n(k_1 r)$ and $N_n(k_1 r)$ are Bessel and Neumann functions of order n, respectively. $\mathbf{i}_r$, $\mathbf{i}_\phi$ and $\mathbf{i}_z$ are unit vectors of the cylindrical coordinate system (r, ϕ, z). $\{A_n\}$–$\{D_n\}$, $\{F_n\}$, $\{G_n\}$, $\{K_n\}$ and $\{L_n\}$ are unknown coefficients.

In terms of Eqs. (1)–(9) and Maxwell's equations, the magnetic field within the cavity $\mathbf{H}^d$ is expressed as

$$\mathbf{H}^d = \sum_{n=0}^{N} (H_{rn}^d \mathbf{i}_r + H_{\phi n}^d \mathbf{i}_\phi) \quad (10)$$

In Region 1 $\quad (a_1 \le r \le d_0)$

$$H_{rn}^d = \frac{-jn}{\omega\mu_0 r} [\{A_n J_n(k_1 r) + B_n N_n(k_1 r)\} \sin(n\phi) - \{C_n J_n(k_1 r) + D_n N_n(k_1 r)\} \cos(n\phi)] \quad (11)$$

$$H_{\phi n}^d = \frac{-jk_1}{\omega\mu_0} [\{A_n J_n'(k_1 r) + B_n N_n'(k_1 r)\} \cos(n\phi) + \{C_n J_n'(k_1 r) + D_n N_n'(k_1 r)\} \sin(n\phi)] \quad (12)$$

In Region 2 $\quad (d_0 \le r \le a_0)$

$$H_{rn}^d = \frac{-jn}{\omega\mu_0 r} [\{F_n J_n(k_1 r) + G_n N_n(k_1 r)\} \sin(n\phi) - \{K_n J_n(k_1 r) + L_n N_n(k_1 r)\} \cos(n\phi)] \quad (13)$$

$$H_{\phi n}^d = \frac{-jk_1}{\omega\mu_0} [\{F_n J_n'(k_1 r) + G_n N_n'(k_1 r)\} \cos(n\phi) + \{K_n J_n'(k_1 r) + L_n N_n'(k_1 r)\} \sin(n\phi)] \quad (14)$$

where the prime denotes the derivative with respect to the argument.

The unknown coefficients are determined from the boundary conditions between regions 1 and 2 ($r = d_0$),

$$E_{z\,(region1)}^d = E_{z\,(region2)}^d \quad \text{or} \quad H_{r\,(region1)}^d = H_{r\,(region2)}^d \quad (15)$$

$$H_{\phi\,(region2)}^d - H_{\phi\,(region1)}^d = \frac{I_0}{d_0} \delta(\phi - \phi_0), \quad (16)$$

and the impedance boundary conditions at aperture 1,

$$\sum_{n=0}^{N} \{y_n^{cJ}(1) E_{zn}^{cJ} + y_n^{cN}(1) E_{zn}^{cN} + y_n^{sJ}(1) E_{zn}^{sJ} + y_n^{sN}(1) E_{zn}^{sN} + H_{tn}^{cJ}(1,2) + H_{tn}^{cN}(1,2) + H_{tn}^{sJ}(1,2) + H_{tn}^{sN}(1,2)\} - H_t^d = 0, \quad (17)$$

and at aperture 2,

$$-\sum_{n=0}^{N} \{y_n^{cJ}(2) E_{zn}^{cJ} + y_n^{cN}(2) E_{zn}^{cN} + y_n^{sJ}(2) E_{zn}^{sJ} + y_n^{sN}(2) E_{zn}^{sN} + H_{tn}^{cJ}(2,1) + H_{tn}^{cN}(2,1) + H_{tn}^{sJ}(2,1) + H_{tn}^{sN}(2,1)\} - H_t^d = 0. \quad (18)$$

I_0 is the total current at the feed point. $H_{tn}^p(i,j)$ indicates the magnetic field at aperture i produced by

the magnetic current $M_n^p(j)$ at aperture j. The superscript p expresses cJ, cN, sJ and sN. The superscripts cJ, cN, sJ and sN in $H_{tn}(i,j)$ mean the magnetic fields corresponding to electric fields E_{zn}^{cJ}, E_{zn}^{cN}, E_{zn}^{sJ} and E_{zn}^{sN}, respectively. $y_n^p(i)$ is the self-admittance of order n at aperture i and is defined by Eq. (28) in the next section. H_t^d is given by

$$H_t^d = \mathbf{H}^d \cdot \mathbf{t} = \sum_{n=0}^{N} (H_{rn}^d \mathbf{i}_r + H_{\phi n}^d \mathbf{i}_\phi) \cdot \mathbf{t}. \tag{19}$$

Since the geometry of the patch does not coincide with the coordinate system (r, ϕ, z), the impedance boundary conditions (17) and (18) are applied in the sense of the least squares [12]. Rearranging Eqs. (17) and (18) in terms of the coefficients $\{F_n\}$, $\{G_n\}$, $\{K_n\}$ and $\{L_n\}$, the impedance boundary conditions are summarized as

$$\begin{aligned} T = \int_C \Bigg| \sum_{n=0}^{N} \{ & F_n f_n(t) + G_n g_n(t) + K_n k_n(t) \\ & + L_n l_n(t) + i_n(t) \} \Bigg|^2 dt \ \rightarrow \ \text{minimum}. \end{aligned} \tag{20}$$

Integration interval C is the circumference of the apertures. t represents any position at the apertures. $f_n(t)$, $g_n(t)$, $k_n(t)$, $l_n(t)$ and $i_n(t)$ are derived from Eqs. (17) and (18) straightforwardly and expressed in terms of Bessel, Neumann and trigonometric functions. The unknown coefficients $\{F_n\}$, $\{G_n\}$, $\{K_n\}$ and $\{L_n\}$ in Eq. (20) are obtained by the simultaneous equations

$$\begin{aligned} \frac{\partial T}{\partial {F_n}^*} = & \sum_{m=0}^{N} [F_m({f_n}^*, f_m) + G_m({f_n}^*, g_m) \\ & + K_m({f_n}^*, k_m) + L_m({f_n}^*, l_m) \\ & + ({f_n}^*, i_m)] = 0, \quad n = 0, 1, 2, \ldots, N \end{aligned} \tag{21}$$

$$\begin{aligned} \frac{\partial T}{\partial {G_n}^*} = & \sum_{m=0}^{N} [F_m({g_n}^*, f_m) + G_m({g_n}^*, g_m) \\ & + K_m({g_n}^*, k_m) + L_m({g_n}^*, l_m) \\ & + ({g_n}^*, i_m)] = 0, \quad n = 0, 1, 2, \ldots, N \end{aligned} \tag{22}$$

$$\begin{aligned} \frac{\partial T}{\partial {K_n}^*} = & \sum_{m=0}^{N} [F_m({k_n}^*, f_m) + G_m({k_n}^*, g_m) \\ & + K_m({k_n}^*, k_m) + L_m({k_n}^*, l_m) \\ & + ({k_n}^*, i_m)] = 0, \quad n = 0, 1, 2, \ldots, N \end{aligned} \tag{23}$$

$$\begin{aligned} \frac{\partial T}{\partial {L_n}^*} = & \sum_{m=0}^{N} [F_m({l_n}^*, f_m) + G_m({l_n}^*, g_m) \\ & + K_m({l_n}^*, k_m) + L_m({l_n}^*, l_m) \\ & + ({l_n}^*, i_m)] = 0, \quad n = 0, 1, 2, \ldots, N. \end{aligned} \tag{24}$$

The inner product $({f_n}^*, g_m)$ is defined as

$$({f_n}^*, g_m) = \int_C {f_n}^*(t) g_m(t) dt, \tag{25}$$

where ${f_n}^*$ represents the complex conjugate of f_n.

3. Wall Admittance of Arbitrarily Shaped Microstrip Antenna

Applying the equivalence theorem to the cavity, the equivalent magnetic current $\mathbf{M}$ at the aperture is expressed as

$$\begin{aligned} \mathbf{M} &= \mathbf{E}^d \times \mathbf{n} = E_z^d \mathbf{i}_z \times \mathbf{n} \\ &= \sum_{n=0}^{N} \{ M_n^{cJ}(i) + M_n^{sJ}(i) \\ &\quad + M_n^{cN}(i) + M_n^{sN}(i) \} \mathbf{t}, \end{aligned} \tag{26}$$

$$M_n^p(i) = \begin{cases} -E_{zn}^p : & \text{aperture 1 } (i = 1) \\ E_{zn}^p : & \text{aperture 2 } (i = 2), \end{cases} \tag{27}$$

where the superscript p indicates cJ, sJ, cN and sN. In order to obtain the wall admittance of an arbitrarily shaped MSA easily, the patch is divided into short straight segments and magnetic currents at the apertures are approximated by the superposition of the piecewise triangle functions [13]. From the continuity condition on the tangential component of the magnetic field on the aperture, the wall admittance $y_n^p(i)$ at any point on the aperture is defined by the magnetic field $H_{tn}^p(i,i)$ produced by the equivalent magnetic current $M_n^p(i)$ on the aperture i,

$$y_n^p(i) = -\frac{H_{tn}^p(i,i)}{M_n^p(i)}. \tag{28}$$

The local coordinate system (X, Y, Z) with the origin located at any point of the aperture on the ground plane $z = 0$ is used in order to derive the tangential component of the magnetic field on the aperture. The local coordinate system is shown in Fig. 2. The positive X direction is defined by the tangential t direction. Unit vectors of the local coordinate system (X, Y, Z) are $\mathbf{i}_X, \mathbf{i}_Y$ and $\mathbf{i}_Z$. Since the thickness of the substrate is assumed to be much smaller than the wavelength, the patch may be neglected in the externally equivalent problem. The magnetic field H_{tn}^p produced by the equivalent magnetic current $M_n^p \mathbf{t}$ is expressed by applying the transverse potential to the vector potential

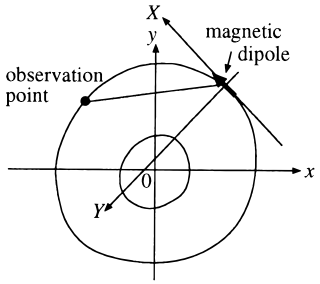

Fig. 2 Local coordinate system with origin located at antenna aperture.

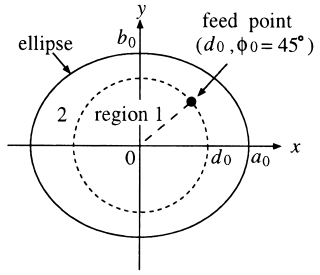

Fig. 3 Geometry of elliptical patch.

[10],

$$H_{tn}^{p} = -j\omega \int_S \mathbf{t} \cdot (\mathbf{i}_X G_F^{XX} + \mathbf{i}_Y G_F^{YX}) M_n^p dS' + \frac{1}{j\omega} \int_S \mathbf{t} \cdot (\nabla G_V)(\nabla' \cdot M_n^p \mathbf{t}) dS'. \quad (29)$$

S denotes the surfaces on the apertures. G_F^{XX} and G_F^{YX} are X and Y components of Green's function for the vector potential due to the X-directed magnetic dipole, respectively. G_V is Green's function for the scalar potential. ∇ and ∇' are the derivative operators at the observation and source points, respectively. Green's functions G_F^{XX}, G_F^{YX} and G_V are obtained by spectral domain analysis [9].

4. Results and Discussion

4.1 Elliptical Microstrip Antenna

Figure 3 shows the geometry and coordinate system of the elliptical MSA. The semimajor axis of the ellipse is a_0 and its semiminor axis is b_0. The antenna is excited at $\phi_0 = 45°$ from the semimajor axis by a coaxial feeder through the dielectric substrate. Substituting $\{B_n\} = 0$ and $\{D_n\} = 0$ into Eqs. (2)–(5), (11) and (12), the electromagnetic fields within the cavity are obtained. Substituting $H_{tn}^{cJ}(2,1) = 0$, $H_{tn}^{cN}(2,1) = 0$, $H_{tn}^{sJ}(2,1) = 0$ and $H_{tn}^{sN}(2,1) = 0$ into Eq. (18), the impedance boundary conditions are obtained.

Figures 4(a) and (b) show the wall conductances g_1^{cJ} and g_1^{sJ} and the wall susceptances b_1^{cJ} and b_1^{sJ} of the first mode on the elliptical MSA, respectively. y_1^{cN} and

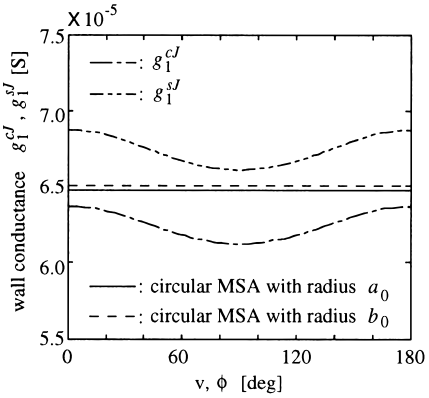

(a) Wall conductances

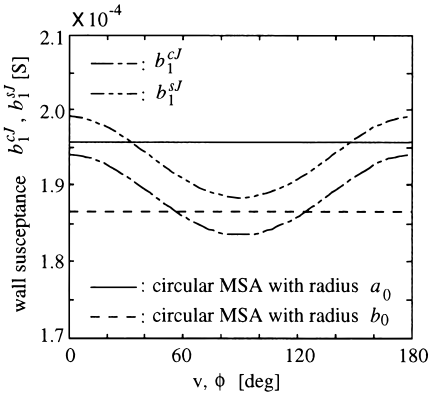

(b) Wall susceptances

Fig. 4 Wall admittances of first mode on elliptical MSA (a_0 = 9.0 mm, b_0/a_0 = 0.97, h = 0.764 mm, ε_r = 2.15, frequency=6.5 GHz).

y_1^{sN} are the same as y_1^{cJ} and y_1^{sJ}, respectively. When the number of segments per wavelength of the magnetic current is around 32, the magnetic fields at the apertures produced by the magnetic currents converge. In these figures, the wall admittances of the circular MSAs with radii a_0 and b_0 are also shown for comparison [9]. The elliptic coordinate system (u_0, v, z) is used on the aperture.

$$u_0 = \tanh^{-1}\left(\frac{b_0}{a_0}\right) \quad (30)$$

$$v = \tan^{-1}\left(\frac{a_0}{b_0}\tan\phi\right) \quad (31)$$

Although the wall admittances of the circular MSA are constant along the circumference, those of the elliptical MSA depend on the distance from the origin. The contributions to the magnetic fields from the magnetic currents M_1^{cJ} and M_1^{sJ} at the aperture of the elliptical MSA are different from those of the circular MSAs with radii a_0 and b_0, respectively. Therefore, y_1^{cJ} at $\phi = 0°$ and y_1^{sJ} at $\phi = 90°$ do not coincide with the wall admittances of the circular MSAs with radii a_0 and b_0,

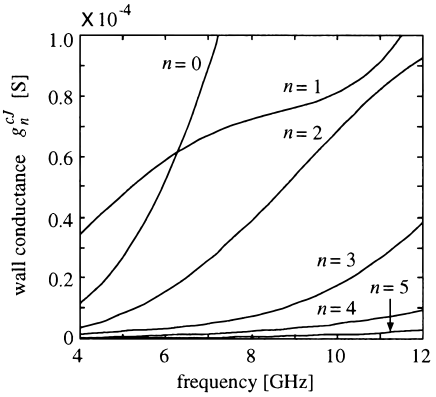

(a) Wall conductances

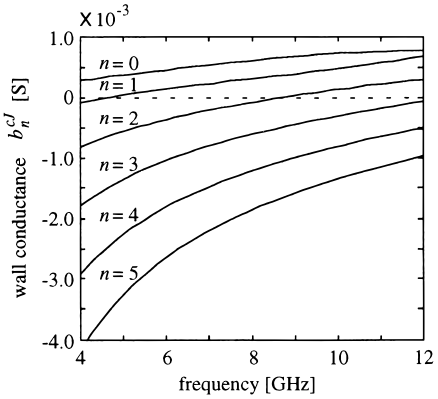

(b) Wall susceptances

Fig. 5 Wall admittances of elliptical MSA at $v = 0°$ ($a_0 = 9.0\,\text{mm}$, $b_0/a_0 = 0.97$, $h = 0.764\,\text{mm}$, $\varepsilon_r = 2.15$).

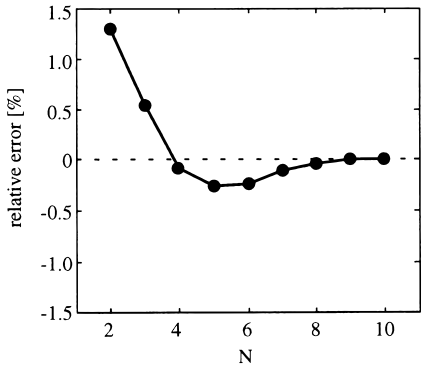

Fig. 6 Relative errors of electric field of elliptical MSA at $v = 0°$ ($a_0 = 9.0\,\text{mm}$, $b_0/a_0 = 0.97$, $d_0 = 6.0\,\text{mm}$, $h = 0.764\,\text{mm}$, $\varepsilon_r = 2.15$, frequency = 6.5 GHz).

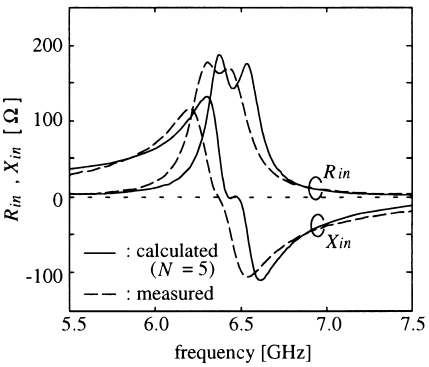

Fig. 7 Input impedance of elliptical MSA ($a_0 = 9.06\,\text{mm}$, $b_0/a_0 = 0.97$, $d_0 = 6.33\,\text{mm}$, $h = 0.764\,\text{mm}$, $\varepsilon_r = 2.15$, $\tan\delta = 0.001$).

respectively. Similarly, the difference between y_1^{cJ} and y_1^{sJ} is due to the difference of the contributions to the magnetic fields from the magnetic currents M_1^{cJ} and M_1^{sJ}.

Figures 5(a) and (b) show g_n^{cJ} and b_n^{cJ} at $v = 0°$ on the aperture, respectively. These wall conductances include the surface wave conductance [9]. The wall conductances decrease as the mode becomes higher. Therefore, the sum of the radiation loss and the surface wave loss of the higher order modes is smaller than that of the lower order modes. The wall susceptances of the lower order modes are positive and those of the higher order modes are negative around the resonant frequency 6.5 GHz. This indicates that the fringe fields of the lower order modes in the neighborhood of the aperture are capacitive and those of the higher order modes are inductive.

The relative error of the electric field within the cavity is defined as

$$\text{relative error} = \frac{|\,I_N\,| - |\,I_{10}\,|}{|\,I_{10}\,|} \times 100\ [\%], \qquad (32)$$

where

$$I_N = \left| \sum_{n=0}^{N} E_{zn}^{d}(a_0, 0) \right|. \qquad (33)$$

The calculated electric fields within the cavity become stationary as N is increased from 10 to 15. Therefore, the electric field at $N = 10$ is used as the reference value. Figure 6 shows the relative error of the elliptical MSA. When $N \geq 5$, the relative error is less than 0.3%. When the geometry of the elliptical patch is slightly different from that of a circle, circularly polarized waves are radiated. Therefore, the calculated electric field quickly converges for N.

Figure 7 shows the calculated and measured input impedances of the elliptical MSA. The input impedance is derived from Poynting's theorem in order to consider the conductor loss and dielectric loss which are not included in the cavity model [9]. Moreover, the calculated input impedance includes the surface wave loss in addition to the radiation loss. The antenna is made of copper-clad glass-fiber PTFE. The calculated input impedance agrees fairly well with the measured data. The relative error of the measured resonant frequency to the calculated one is 1.4%.

Figure 8 shows the calculated and measured axial

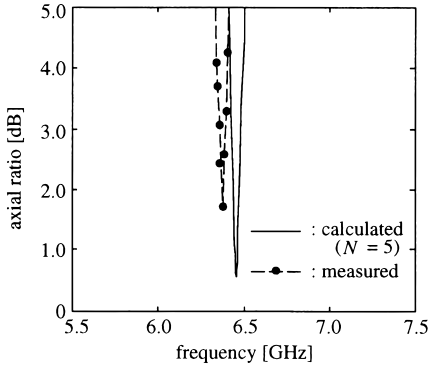

Fig. 8 Axial ratio of elliptical MSA ($a_0 = 9.06\,\text{mm}$, $b_0/a_0 = 0.97$, $d_0 = 6.33\,\text{mm}$, $h = 0.764\,\text{mm}$, $\varepsilon_r = 2.15$, $\tan\delta = 0.001$).

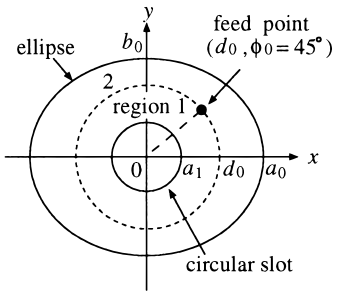

Fig. 9 Geometry of elliptical patch with a circular slot.

ratios of the elliptical MSA. The calculated minimum axial ratio is 0.6 dB at 6.46 GHz and the measured value is 1.7 dB at 6.38 GHz.

4.2 Elliptical Microstrip Antenna with a Circular Slot

Figure 9 shows the geometry and coordinate system of the elliptical MSA with a circular slot. The semimajor axis of the ellipse is a_0, its semiminor axis is b_0 and the radius of the circular slot is a_1. The antenna is fed at $\phi_0 = 45°$ from the semimajor axis.

Figures 10(a) and (b) show the self-conductances g_1^{cJ} and g_1^{sJ} and the self-susceptances b_1^{cJ} and b_1^{sJ} of the first mode, respectively. The self-admittances at the outer aperture vary depending on the observation point and the magnetic current distributions. The self-susceptances at the outer aperture are capacitive and those at the inner aperture are inductive.

Figure 11 shows the absolute values of the magnetic fields of the first mode on the apertures. Since $|H_1^{cJ}(1,2)|$ is about 20% of $|H_1^{cJ}(1,1)|$, the mutual coupling between the outer aperture and the inner slot cannot be neglected in the calculation.

The left-hand side of Eq. (17) denotes $H_\phi^e - H_\phi^d$. The relative error of the real part at aperture 1 is defined as

$$\text{relative error} = \frac{\text{real part } (H_\phi^e - H_\phi^d)}{\text{maximum value of real part } (H_\phi^e)} \times 100\ [\%]. \tag{34}$$

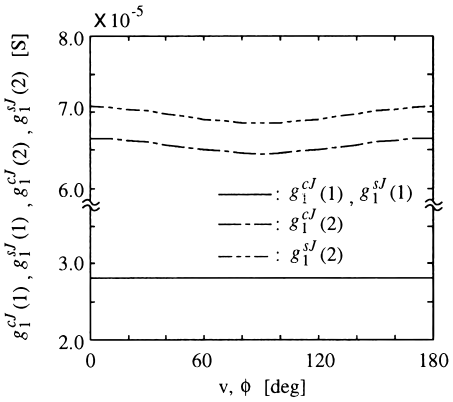

(a) Self-conductances

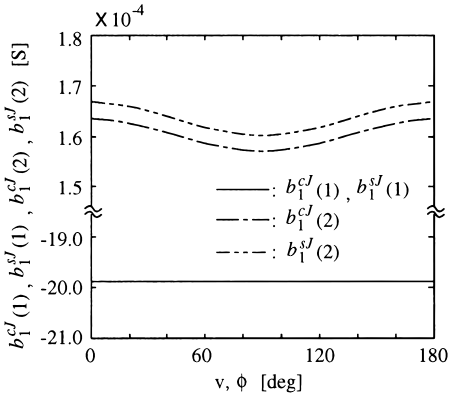

(b) Self-susceptances

Fig. 10 Self-admittances of first mode on elliptical MSA with a circular slot ($a_0 = 8.04\,\text{mm}$, $b_0/a_0 = 0.98$, $a_1 = 2.02\,\text{mm}$, $h = 0.764\,\text{mm}$, $\varepsilon_r = 2.15$, frequency = 6.7 GHz).

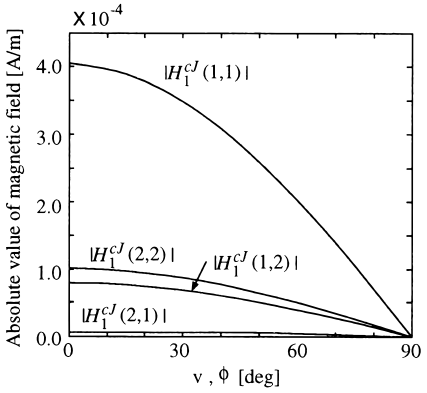

Fig. 11 Magnetic fields at aperture of elliptical MSA with a circular slot ($a_0 = 8.04\,\text{mm}$, $b_0/a_0 = 0.98$, $a_1 = 2.02\,\text{mm}$, $d_0 = 6.0\,\text{mm}$, $h = 0.764\,\text{mm}$, $\varepsilon_r = 2.15$, frequency = 6.7 GHz).

Similarly, the relative error of the imaginary part at aperture 1 and those at aperture 2 are defined. Figures 12(a) and (b) show the relative errors of boundary conditions (17) and (18), respectively. As the relative errors oscillate along the circumferences, the integral of the magnetic field satisfies the boundary conditions [14]. Since the electromagnetic fields at the elliptical

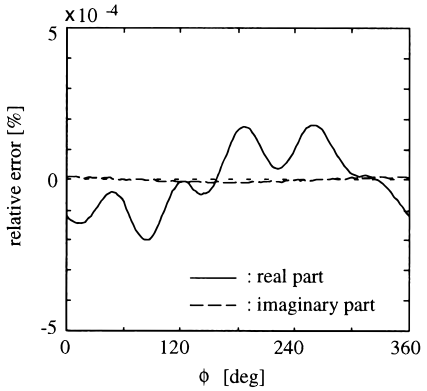

(a) Aperture 1

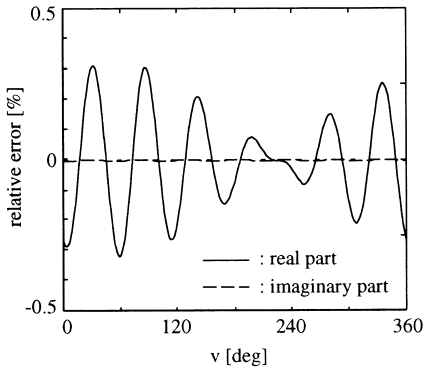

(b) Aperture 2

Fig. 12 Relative errors of boundary conditions (17) and (18) on elliptical MSA with a circular slot ($a_0 = 8.04\,\text{mm}$, $b_0/a_0 = 0.98$, $a_1 = 2.02\,\text{mm}$, $h = 0.764\,\text{mm}$, $\varepsilon_r = 2.15$, $N = 5$, frequency = 6.7 GHz).

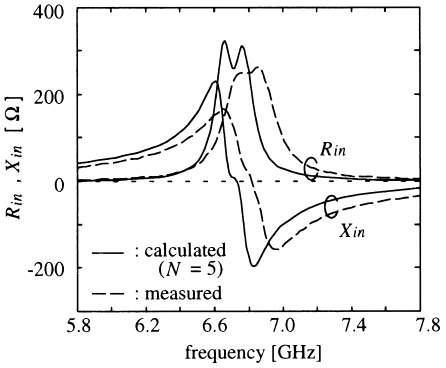

Fig. 13 Input impedance of elliptical MSA with a circular slot ($a_0 = 8.04\,\text{mm}$, $b_0/a_0 = 0.98$, $a_1 = 2.02\,\text{mm}$, $d_0 = 6.0\,\text{mm}$, $h = 0.764\,\text{mm}$, $\varepsilon_r = 2.15$, $\tan\delta = 0.001$).

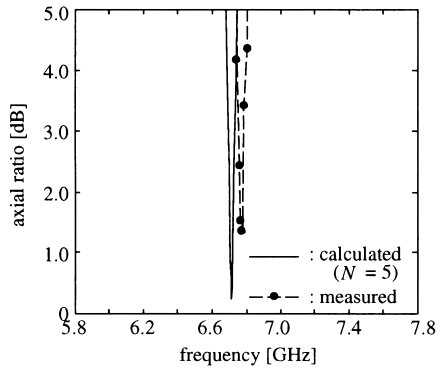

Fig. 14 Axial ratio of elliptical MSA with a circular slot ($a_0 = 8.04\,\text{mm}$, $b_0/a_0 = 0.98$, $a_1 = 2.02\,\text{mm}$, $d_0 = 6.0\,\text{mm}$, $h = 0.764\,\text{mm}$, $\varepsilon_r = 2.15$, $\tan\delta = 0.001$).

aperture are expressed by the cylindrical coordinate system, the relative errors at aperture 2 are bigger than those at aperture 1.

Figures 13 and 14 show the calculated and measured input impedances and axial ratios of the elliptical MSA with a circular slot, respectively. The relative error of the measured resonant frequency to the calculated one is 1.7%. The calculated minimum axial ratio is 0.24 dB at 6.72 GHz and the measured value is 1.35 dB at 6.78 GHz. The calculated results agree fairly well with the measured data.

5. Conclusion

The wall admittance of the arbitrarily shaped MSA has been generally formulated, and the elliptical MSAs with and without a circular slot are calculated. The wall admittance is defined by the magnetic field produced by the equivalent magnetic current on the aperture. The magnetic fields have been derived using Green's functions obtained by the spectral domain analysis. In the spectral domain analysis, the outside region of the cavity is modeled as a layered medium consisting of the free space, the dielectric substrate with a magnetic dipole and the ground plane.

Although the wall admittances are constant in the circular slot, those at the elliptical aperture vary depending on the observation point and the magnetic current distributions. The wall susceptances of the lower order modes on the elliptical MSA are capacitive and those of the higher order modes are inductive around the resonant frequency. This indicates that the fringe fields of the lower order modes in the neighborhood of the aperture are capacitive and those of the higher order modes are inductive. The self-susceptances of the first mode on the elliptical MSA with a circular slot become capacitive at the outer aperture and inductive at the inner aperture.

In this paper, the cavity model has been extended to the MSA with a patch whose geometry deviates from a particular coordinate system. The electromagnetic fields within the cavity of elliptical MSAs with and without a circular slot are expanded in terms of the eigenfunctions in the cylindrical coordinate system and their expansion coefficients are determined by applying the impedance boundary condition at the apertures in the sense of the least squares. The calculated input impedance and axial ratio of the elliptical MSAs with

and without a circular slot agree fairly well with the experimental data. The relative errors of the measured frequencies at resonance and minimum axial ratio to the calculated ones are almost the same. This error is due to the assumption that the electromagnetic fields within the cavity are uniform in the z direction [9].

Acknowledgement

The input impedances of MSA were measured at the Joint Research and Development Center, Saga University. The authors would like to thank Research Associate E. Nishiyama of Saga University for his valuable advice on the measurement of MSA. This research was supported in part by a Grant-in-Aid for Scientific Research (09750429) from the Ministry of Education, Science, Sports and Culture of Japan.

References

[1] Y.T. Lo, D. Solomon, and W.F. Richards, "Theory and experiment on microstrip antennas," IEEE Trans. Antennas & Propag., vol.AP-27, no.2, pp.137–145, March 1979.
[2] A.K. Bhattacharyya and R. Garg, "Generalised transmission line model for microstrip patches," Proc. IEE, vol.132, Pt.H, no.2, pp.93–98, April 1985.
[3] A.G. Derneryd, "Linearly polarized microstrip antennas," IEEE Trans. Antennas & Propag., vol.AP-24, no.6, pp.846–851, Nov. 1976.
[4] K.R. Carver and J.W. Mink, "Microstrip antenna technology," IEEE Trans. Antennas & Propag., vol.AP-29, no.1, pp.2–24, Jan. 1981.
[5] L.C. Shen, "Analysis of circular-disc printed-circuit antenna," Proc. IEE, vol.126, no.12, pp.1220–1222, Dec. 1979.
[6] S. Yano and A. Ishimaru, "Theoretical study of the input impedance of circular microstrip disk antenna," IEEE Trans. Antennas & Propag., vol.AP-29, no.1, pp.77–83, Jan. 1981.
[7] A.K. Bhattacharyya and R. Garg, "Spectral domain analysis of wall admittances for circular and annular microstrip patches and the effect of surface waves," IEEE Trans. Antennas & Propag., vol.AP-33, no.10, pp.1067–1073, Oct. 1985.
[8] A.K. Bhattacharyya and R. Garg, "Input impedance of annular ring microstrip antenna using circuit theory approach," IEEE Trans. Antennas & Propag., vol.AP-33, no.4, pp.369–374, April 1985.
[9] T. Fujimoto, K. Tanaka, and M. Taguchi, "Wall admittance of circular microstrip antenna," IEICE Trans. Commun., vol.E82-B, no.5, 760–767, May 1999.
[10] J.R. Mosig, "Integral equation technique," in Numerical techniques for microwave and millimeter-wave passive structures, ed. T. Itoh, pp.133–213, John Wiley & Sons, New York, 1989.
[11] L.C. Shen, "The elliptical microstrip antenna with circular polarization," IEEE Trans. Antennas & Propag., vol.AP-29, no.1, pp.90–94, Jan. 1981.
[12] H. Ikuno and K. Yasuura, "Improved point-matching method with application to scattering from a periodic surface," IEEE Trans. Antennas & Propag., vol.AP-21, no.5, pp.657–662, Sept. 1973.
[13] T. Mizuguchi, T. Fujimoto, K. Tanaka, and M. Taguchi, "Surface admittance of rectangular microstrip antenna," IEICE Technical Report, AP96-128, Jan. 1997.
[14] S. Egashira, M. Taguchi, and H. Kitajima, "The effect of the end surface current on the numerical solution of wire antennas," IECE Trans., vol.J68-B, no.6, pp.714–721, June 1985.

Takafumi Fujimoto received his B.E. and M.E. degrees from Nagasaki University in 1992 and 1994, respectively. He is currently a Research Associate at Nagasaki University. His main interests have been the analytical method of microstrip antennas and the active antenna.

Kazumasa Tanaka received his B.S., M.S. and Dr.E. degrees in Electronic Communication Engineering, in 1965, 1967, and 1975, respectively, all from Kyushu University, Japan. Since 1981, he has been a professor at Nagasaki University. His main areas of interest are the diffraction of optical beams, the detection of optical signals, and optical engineering. Dr. Tanaka is a member of the Japan Society of Applied Physics and Optical Society of America.

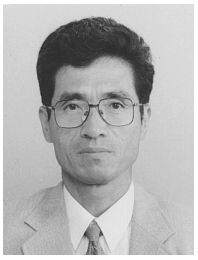

Mitsuo Taguchi received his B.E. and M.E. degrees from Saga University in 1975 and 1977, respectively, and a Dr.Eng. degree from Kyushu University in 1986. From 1977 to 1987, he was a Research Associate at Saga University. Since 1987 he has been an Associate Professor at Nagasaki University. In 1996 he was a Visiting Scholar at the Department of Electrical Engineering at the University of California, Los Angeles. His research interests are the active antennas, the microstrip antennas, and the linear antennas. Dr. Taguchi is a member of the IEEE and the Institute of Image Information and Television Engineers.